Quantum-Well-Detector Concept for Hyperspectral, Coregistered Full-Stokes-Vector Detection

Mario Serna

Air Force Research Labs, Space Vehicle Directorate
3550 Aberdeen Ave SE, Kirtland AFB, NM 87117-5776, USA

ABSTRACT

By layering quantum well stacks separated by partially transmissive linear gratings, similar to a multi-color QWIP, one may be able to detect the full Stokes vector at a single pixel. Such a detector would greatly aid polarization-based automated algorithms to detect targets from earth-gazing platforms. We report results from a theoretical calculation of normally incident infrared light absorbed by quantum wells in an eight-layer quantum-well/grating structure. The structure, illuminated from the substrate, consists of four quantum-well stacks, of 50 quantum wells each, separated by contact layers and lamellar gratings. The gratings following the first three quantum well stacks are formed by perfectly conducting rectangular strips separated by a transparent dielectric that allows some light to be transmitted. The top grating, following the fourth quantum well stack, is completely reflective. Each of the four lamellar gratings is oriented at a different angle. Incident radiation is diffracted and reflected to different orders and at different angles at each of the four gratings. The model is based on a uniaxial-optics transfer-matrix technique. We calculate the energy absorbed by each of the layers. This in turn allows one to predict and compare which layers will respond for partially- and fully-polarized incident light of either linear or circular polarization.

Keywords: Polarimeter, coregistered, Stokes vectors, snapshot, polarization uncertainty, pixel

1. BACKGROUND ON IMAGING POLARIMETERS

Polarimetric imaging has more information than intensity imaging and improves remote sensing and automatic target recognition.[1] Polarimetry can be used to identify materials and to distinguish samples from a cluttered background.[2] Polarimetry has also shown promise for mine detection.[3] On average, polarimetric images of man-made objects have a higher degree of polarization (DOP) than polarimetric images of natural objects. This pattern may be useful for spectro-polarimetric sub-pixel target detection. Polarimetric data is often represented in terms of Stokes parameters.

The four Stokes parameters,[4] which represent all the polarization information, are: $S_0 = I_0 + I_{90}$, $S_1 = I_0 - I_{90}$, $S_2 = I_{45} - I_{135}$, and $S_3 = I_R - I_L$ where I_X is the measured intensity of the light after passing through a linear filter at an orientation of X degrees, and I_R and I_L are the measured intensities of the right or left circularly polarized fraction of the light. The DOP, in terms of Stokes parameters, is given by $DOP = \sqrt{S_1^2 + S_2^2 + S_3^2}/S_0$.

Imaging polarimeters typically collect several images with several filters. One design uses a rotating quarter-wave plate with a linear filter.[2] With a single focal plane, the device takes several images at different rotations of the polarizing filters. The appropriate images are averaged and subtracted to extract the four Stokes parameters at each pixel. Because the images were separated in time, any motion in the scene will manifest as erroneous polarization. This erroneous polarization precludes use from moving plantforms, such as airborne or spaceborne sensors, or imaging moving targets. Another design uses four separate cameras with different polarization filters. The four cameras take simultaneous images; the appropriate images are added and subtracted to extract the four Stokes parameters. Parallax or camera misalignment will manifest as erroneous polarization. At a previous

Send correspondence to Capt. Mario Serna
E-mail: mariojr@alum.mit.edu, Telephone: 1 505 853 7680

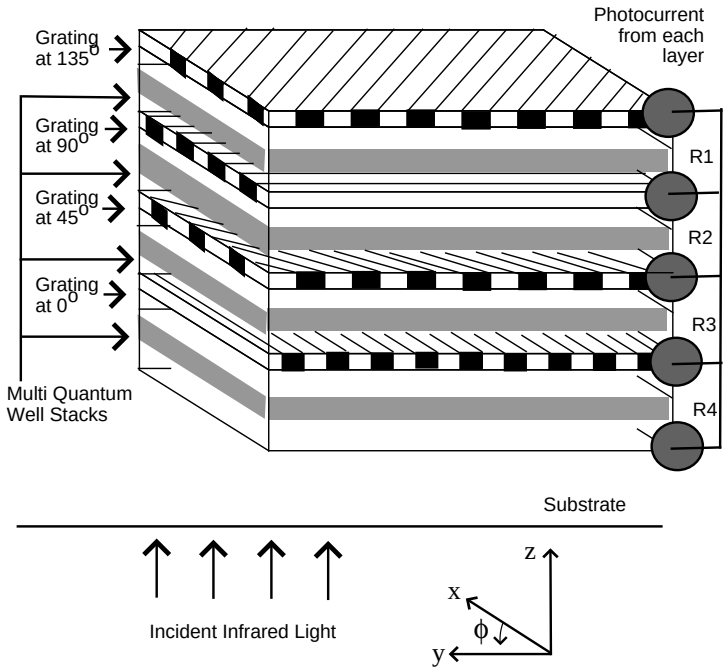

Figure 1. The pixel polarimeter is built by stacking multi quantum well photoconductors and gratings at different orientations. The photocurrent from each layer is read individually.

SPIE, Peterson[5] showed that if pixels detecting the different polarization components are misaligned by 0.01, then images of edges or point sources may have have an DOP error as high as 0.01. A typical pixel of an LWIR (8 - 12 μm) image has a DOP of 0.025; therefore, to maintain a signal to noise of 10:1, the misalignment of the four images may not exceed 0.0025.

Some recent polarimeter designs work to overcome these drawbacks.

Beekman and Van Anda use four spatially separated pixels of a quantum well infrared phototector (QWIPs) camera with linear gratings oriented at 0^o and 90^o to eliminate camera misalignment and parallax.[6] Even with this design, the spatially separated polarimetric pixels manifest as erroneous polarization. In this instance the relative alignment of the pixels is known exactly, but the misalignment between pixels that measure the different polarization fractions is still more than 100% the width of a pixel. This misalignment still results in the large erroneous polarization measurements described by Peterson.[5]

A device invented by P. Kebabian, p-SIM, uses polarimetric interference to encode the polarization information as a modulation of the spectral intensity measured with a pushbroom hyperspectral imager.[7] This design simultaneously detects the polarization and the spectrum over a column of pixels. Polarization features change as rapidly as the index-of-refraction features, which are about 2 μm wide in the LWIR (8-12 μm) and shorter in the visible. The feature size limits the spectral space on which one can encode the polarization. The device's principle of operation leaves ambiguous what wavelength is associated with what polarization and has difficulty detecting circular polarization in a reasonable spectral window.

The device I present in this paper should detect the full-polarization at each pixel, at each frame, and at each wavelength.

2. DEVICE DESCRIPTION AND PRINCIPLE OF OPERATION

The pixel-polarimeter device detects the incident light's polarization by exploiting the polarization-dependent absorption of quantum well infrared photodetectors, the polarization-dependent diffraction from linear grat-

ings, and the polarization-dependent interference of electromagnetic waves. In this section, these conceptual components will be discussed and then synthesized into the pixel-polarimeter.

Quantum wells are semiconductor structures formed by growing layers of GaAs in-between layers of $Al_xGa_{1-x}As$. The GaAs wells extend indefinitely in the x-y plane and about 5 nm in the z-direction (also called the growth direction). The $Al_xGa_{1-x}As$ barriers also extend indefinitely in the x-y plane and about 30 nm in the z-direction. The mismatch between the conduction bands of GaAs and $Al_xGa_{1-x}As$ forms a finite barrier 1-D quantum-well in the conduction band with quantized energy levels E_1, E_2, ... The energy levels can be varied by changing the thickness of the wells or the Al fraction (x) of the barriers. Only the z-polarized component of light with frequency $\hbar\omega = E_2 - E_1$ can optically couple the intersubband energy levels of the quantum-well. This polarization selection rule has been experimentally verified to an accuracy of 0.2%.[8] Quantum-wells do not absorb normally incident light (light that travels in the z-direction) because they have no electric field component in the z-direction.

Stacks of multiple quantum wells (MQWs) are used to build quantum well infrared photodetectors (QWIPs).[9] Electrons in n-doped quantum wells can be photoexcited into the conduction band. When a bias is applied across the wells, these photo-excited electrons increase the current flowing across the device. The photon induced change in current (photocurrent) is a measure of the incident photon flux. Today's commercial QWIPs use gratings to detect normally incident light. Linear gratings diffract the TM-polarized component (the polarization component with the magnetic field transverse, or perpendicular, to the plane of incidence) into diffraction orders ± 1 that can be absorbed by the quantum wells. Linear gratings also diffract the TE-polarized component (the polarization component with the electric field transverse to the plane of incidence) into diffracted orders ± 1, but no TE-polarized light can be absorbed by the quantum wells.

Linear gratings also have polarization-dependent physics. Grating efficiency is different for fast polarization (no magnetic field parallel to the grating's grooves) and slow polarization (no electric field parallel to the grating's grooves).[10, 11] For example, consider light with a 2.5 μm wavelength normally incident on a perfectly conducting grating with a 3 μm period, 1.5 μm grooves, and 0.75 μm depth. The fast polarization will be 14% reflected (into the 0^{th} order) and 43% diffracted into the ± 1 orders, and the slow-polarization will be 30% reflected (into 0^{th} order) and 35% diffracted into the ± 1 orders. Unlike an isotropic dielectric material, linear gratings have polarization dependent reflection and transmission coefficients even at normal incidence. In addition, polarized light incident on a linear grating will have a relative phase shift between the diffracted fast and slow polarization components.[11]

Light diffracted from the four gratings will electromagnetically interfere in the pixel polarimeter. Polarization-dependent interference of electromagnetic waves is a well-known phenomenon.[4] The layers of the pixel-polarimeter are about 2 to 3 μm thin. These layers are about as thick as the wavelength of 10 μm infrared light in GaAs (because $\epsilon_{GaAs} = 10.73$, the wavelength in the material is about 3.05 μm).[12] Interference among the multiple reflections of light between thin dielectric layers is familiar in anti-reflective coatings or Fabry-Perot étalons.

The pixel polarimeter in this paper is based on quantum well infrared photodetector (QWIP) technology.[9] The proposed device, shown in fig. 1, has at least four multi-quantum-well (MQW) stacks separated by linear gratings at different orientations. Infrared light is incident on the pixel from the substrate. Similar to multi-color QWIPs,[13] in each pixel, separate electrical contact is made with each of the four gratings plus the substrate. In order to ensure an ohmic contact between the MQW and the gratings, the semiconductor material surrounding the gratings should be n-doped. The bias across each MQW stack can be adjusted individually, and the photocurrent across each MQW stack will be proportional to the incident flux.

We combine these polarization-dependent phenomena (quantum well absorption, diffraction from the four gratings, and interference among the diffraction paths) to make the relative photocurrent from the four MQW layers polarization dependent. Interference from multiple reflections and transmissions of the z-propagating light modulates the absorption of the ± 1 diffracted orders at each MQW layer. The quantum-wells do not absorb light propagating in the z-direction. The non-absorbed z-propagating light experiences a polarization-dependent reflection and transmission at each grating. Interference among the multiple reflections and transmissions communicates the polarizaiton information into the amount of TM-polarized light diffracted into the ± 1 orders

at each grating. The TM-polarized ±1 orders is absorbed by the quantum wells. In this manner, the relative photocurrent from the four MQW layers becomes polarization-dependent.

Polarization detection is only possible when the light incident on the pixel has a narrow wavelength band. To satisfy this operational requirement the pixel-polarimeter should be employed in combination with a grating spectrometer as a part of a pushbroom diffraction hyperspectral imager. Another option is to use the pixel polarimeter as a snapshot camera in combination a narrow band filter.

The polarization may be extracted using linear algebra. The Stokes vector is a 4-dimensional linear vector space which represents the polarization of the light. The photocurrents from the four readouts also form a vector space that is linear in the four Stokes parameters. From linear algebra, there exists a linear transformation (a matrix) that will map the four components of the Stokes vector to the four photocurrents. The matrix, if it is non-singular, can be inverted to find the four components of the Stokes vector from the four photocurrents.

3. CALIBRATION AND MEASUREMENT UNCERTAINTY

The matrix that maps the four components of the incident light's Stokes vector S^{in} to the four photocurrents R is the device's polarization response matrix (PRM):

$$R_j = \sum_{k=1}^{4} PRM_{jk}\, S_k^{\text{in}}, \tag{1}$$

where the index j runs from 1 to the number of readouts N_R. For full polarimetric detection $N_R \geq 4$ is required. In matrix notation, Eq. (1) is $R = PRM \cdot S$. Both the readouts and the Stokes vectors form linear vector spaces; therefore from linear algebra, the PRM matrix is a change of basis, and the columns of the PRM are four linearly independent Stokes basis vectors. The components of the PRM can be found by modeling the pixel polarimeter's response to polarized and unpolarized radiation. For example: subtracting the readouts R_j^I of unpolarized light from the readouts R_j^V of vertically polarized light gives the components of the 2$^{\text{nd}}$ column of the PRM matrix: $RPM_{j2} = R_j^I - R_j^V = SBV_j^2$ where SBV is a Stokes basis vector.

If $N_R \geq 4$,the PRM represents an over-determined system. The pseudoinverse ,*i.e.* least squares fit, gives the Stokes vector from the device readouts*. The Stokes vector in matrix notation with the pseudoinverse is given by,

$$S^{\text{in}} = (PRM^T \cdot PRM)^{-1} \cdot PRM^T \cdot R, \tag{2}$$

where PRM^T is the transpose of the matrix PRM. I will abbreviate the 4×5 pseudoinverse of the PRM matrix as

$$\overline{PRM}^{-1} \equiv (PRM^T \cdot PRM)^{-1} \cdot PRM^T. \tag{3}$$

From the error propagation formula, the device's ability to distinguish the distinct Stokes vectors is found to be

$$(\delta S_j)^2 = \sum_{k=1}^{N_R} |(\overline{PRM}^{-1})_{jk}|^2\ (\delta R_k)^2 \tag{4}$$

where δS_j is the uncertainty in the j^{th} Stokes vector and δR_k is the uncertainty in the k^{th} readout. If the uncertainty in the different readouts is equal, the device's inherent polarization uncertainty is given by

$$\Lambda_j = \sqrt{\sum_{k=1}^{N_R} |(\overline{PRM}^{-1})_{jk}|^2} \tag{5}$$

Conceptually, the uncertainty in δS_j may be understood as the ability to distinguish two Stokes basis vectors (SBV) on a two-dimensional readout vector space. If the uncertainties in the two dimensions of the readout

*I am grateful to Paul Alsing for reminding me about the pseudoinverse in over-determined systems.

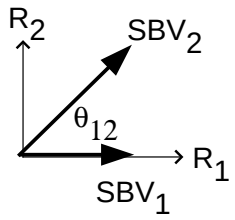

Figure 2. A 2D example of two Stokes basis vectors (SBV_1 and SBV_2) in an orthonormal readout vector space (R_1 and R_2).

space are assumed to be equal, $\delta R = \delta R_1 = \delta R_2$, then the 2×2 inverse can be calculated analytically and gives the uncertainty δS_j to be

$$\delta S_j = \frac{1}{\sin\theta_{12}|SBV_j|}\,\delta R \tag{6}$$

where θ_{12} is the angle between the Stokes basis vectors and $|SBV_j|$ is the length of the Stokes basis vector SBV_j as depicted in fig. 2. The uncertainty in each Stokes vector is found to be inversely proportional to the magnitude of that Stokes basis vector and to the sine of the angle between that Stokes basis vector and the other three Stokes basis vectors.

I now estimate the polarization sensitivity of an actual device. Using current QWIP cameras as a reference,[14] each quantum-well readout can detect changes in photocurrent larger than about 0.02% (this corresponds to an $NE\Delta T$ of $9mK$ for a $300K$ blackbody background). The model that we present in the next section finds a polarization sensitivity of $\Lambda_j \approx 50$ using $N_R = 4$ and moderately optimized device parameters. Using this *Lambda* and $NE\Delta T$, Eq. (6) gives us a polarization uncertainty of about 1.0% per Stokes-vector component.

The polarization sensitivity may be further improved by increasing the parameters in the denominator of Eq. (6). The average angle between Stokes basis vectors may be increased by using $N_R \geq 5$ layers rather than the demonstrated $N_R = 4$. The magnitude of the Stokes basis vector may be increased by using dielectric gratings as opposed to perfectly conducting gratings that we modeled.

4. COMPUTER SIMULATION OF THE PIXEL-POLARIMETER

I constructed a computer simulation of the structure shown in fig. 1. The model requires some constraints on the device parameters to make the problem soluble. The resulting C++ computer code or executable is available upon request.

Each of the linear gratings has a discrete symmetry that shifts the grating by one period d perpendicular to the groove direction $\hat{g}$. Every such discrete symmetry leads to the existence of additional modes related by the reciprocal lattice vector (RLV) $\Delta\vec{k} = 2\pi/d\ (\hat{z} \times \hat{g})$. With four independent gratings and periods the four linearly dependent RLVs combine in any integer multiples to create an infinitely dense set of modes to consider in the model.

In order to limit the density of modes, we constrain the period and orientation of the four gratings to form a repeating unit cell, shown in fig. 3. Each grating has one RLV. Because our four gratings share a repeating unit cell, the RLVs k_B and k_D are formed by $\Delta k_{B(D)} = \Delta k_C + (-)\Delta k_A$.

Using these modes for TE and TM polarized light, we model the device with a transfer matrix method to account for all the polarization-dependent diffraction, interference, and absorption and multiply-scattered light. The grating diffraction efficiency is modeled using a modal expansion technique presented by Anderson and Lundqvist[15] and explained further by Wendler and Kraft[16] and assumes that the gratings are made of perfectly conducting, square, metal strips.

The predicted response of a pixel-polarimeter at $\lambda = 8.42\ \mu m$ is shown in figs. 4 and 5. In both plots, the pixel-polarimeter that is modeled has 50 quantum wells each with peak absorption at $\lambda_{\mathrm{QW}} = 8.42\ \mu m$, well

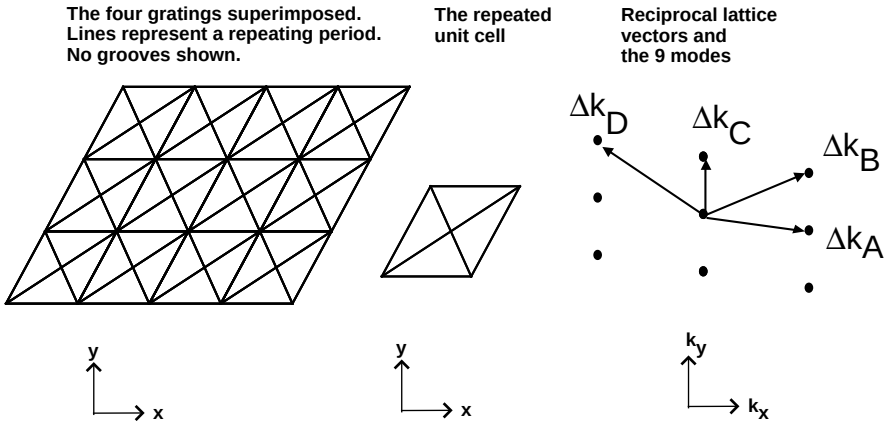

Figure 3. The choice of the grating period and angle for the four layers satisfies a repeating unit cell. This creates a finitely dense set of modes. The model considers only the first 9 modes.

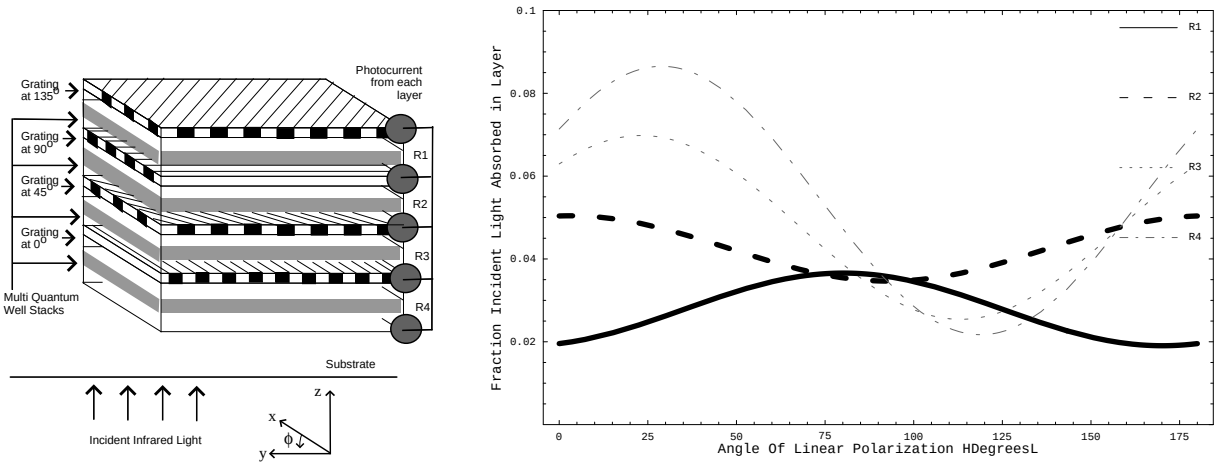

Figure 4. An example of the response from the four layers of the pixel-polarimeter as we rotate the polarization angle of the incident linearly-polarized light.

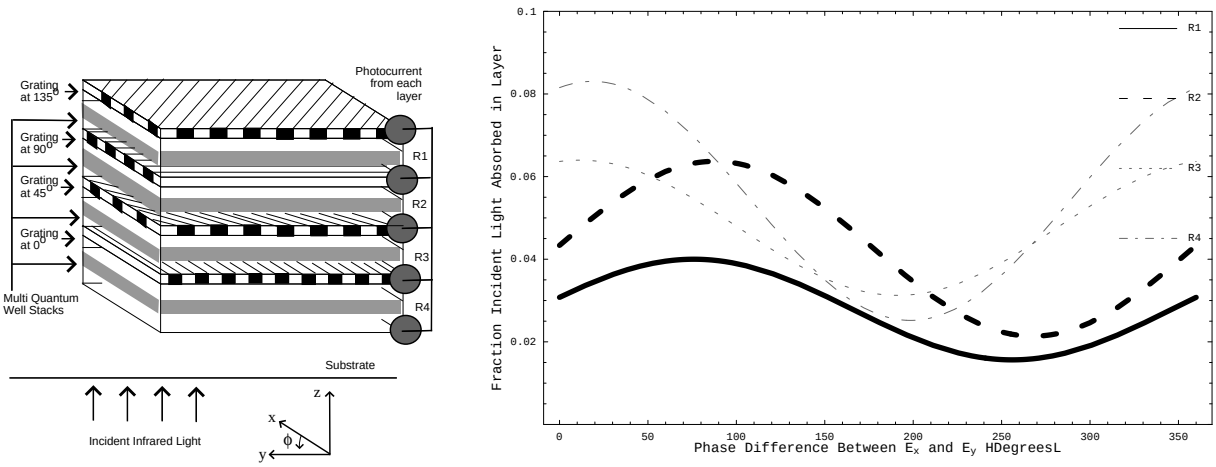

Figure 5. An example of the response from the four layers of the pixel-polarimeter as we vary the phase lag between an x-polarized and y-polarized plane wave.

width of $0.005\mu m$ and barrier width of $0.03\mu m$. The quantum well absorption was modeled with a Drude model, and the Drude model parameters we used were taken from Anderson and Lundqvist's paper.[15] The gratings are structured with orientations as shown in fig. 1. The gratings at 45^o and 135^o have periods of 3.13 μm, and, due to the unit cell, the gratings at 0^o and 90^o have periods of $\sqrt{2} \cdot 3.13\ \mu m = 4.42649\ \mu m$. I refer to the period of the gratings at 45^o and 135^o as the base period. All gratings have depths of 0.3 μm, and duty cycles with GaAs for 0.7 of each period followed by a perfect conductor for 0.3 of the period. The contact layers above and below the gratings are 0.5 μm each.

Fig. 4 shows the linear-polarization responses of the four layers of the pixel polarimeter. The relative response changes as the angle of the linearly-polarized incident light varies. Fig. 5 shows the elliptical-polarization response of the four layers of the pixel polarimeter. The relative response changes as we change the phase lag between an x-polarized and a y-polarized plane wave. Notice that at phase lags of 0^o and 180^o the waves are linearly polarized with angles of 45^o and 135^o respectively.

5. PARAMETER STUDIES

The pixel-polarimeter that we modeled has about 20 design parameters and 20 parameters to describe the physics of the constituent materials and the incident light. In this section, I will show the device's worst case polarization uncertainty factor

$$\Lambda_{\mathrm{WC}} = \frac{1}{\sin\theta_{\min}\,|SBV_{\min}|} \tag{7}$$

as determined by the smallest angle difference between Stokes basis vectors $\theta_{\min}$ and the shortest Stokes basis vector $|SBV_{\min}|$. To keep these scans representative of the scattering physics and independent of the Quantum Well design choices, we set the quantum-well peak-absorption wavelength equal to the wavelength of the incident light.

In figs. 6, 7, and 8, we show the regions of parameter space with reasonable polarization detection performance. The dark regions correspond to parameters for a given incident wavelength where $\Lambda_{\mathrm{WC}} \leq 100$. In these regions for some reasonable QWIP noise and performance, the device can detect DOP changes of 0.02.

Fig. 6 shows how the polarization detection sensitivity changes as I vary the wavelength and the base period of the four gratings. The responses from the four layers shown in figs. 4 and 5 correspond to the parameters of the upper-left dark region of fig. 6.

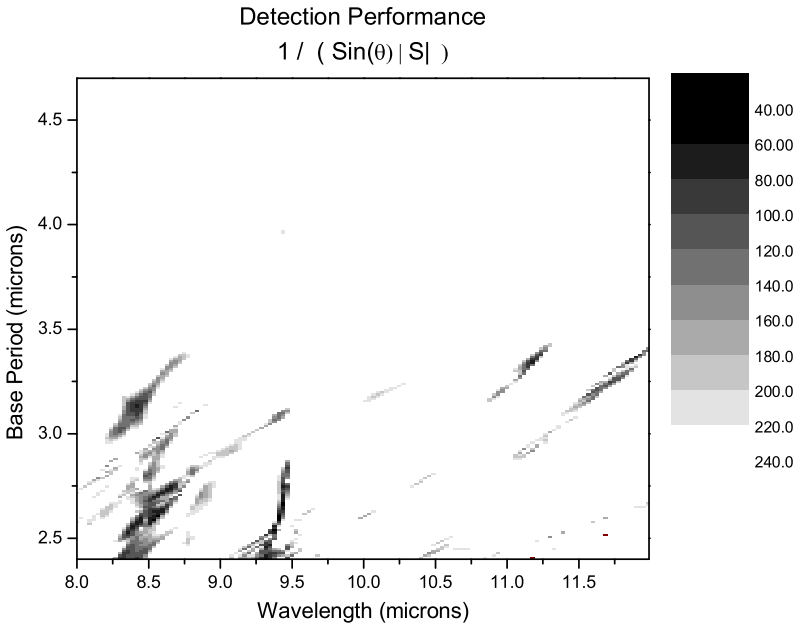

Figure 6. The polarization detection performance for the pixel polarimeter as one varies the wavelength and the base period.

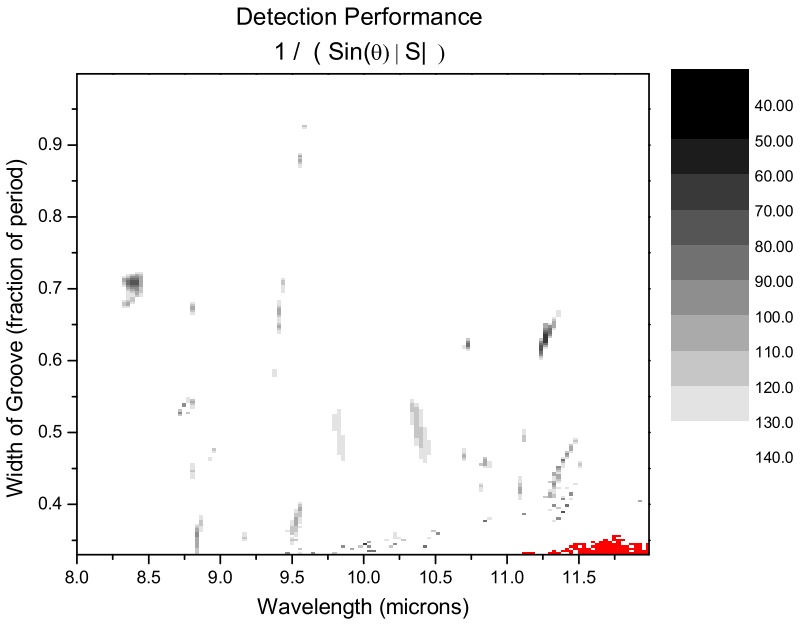

Figure 7. The polarization detection performance for the pixel polarimeter as one varies the wavelength and the size of the dielectric grooves that form the grating. The code becomes unstable for large wavelengths and narrow dielectric grooves.

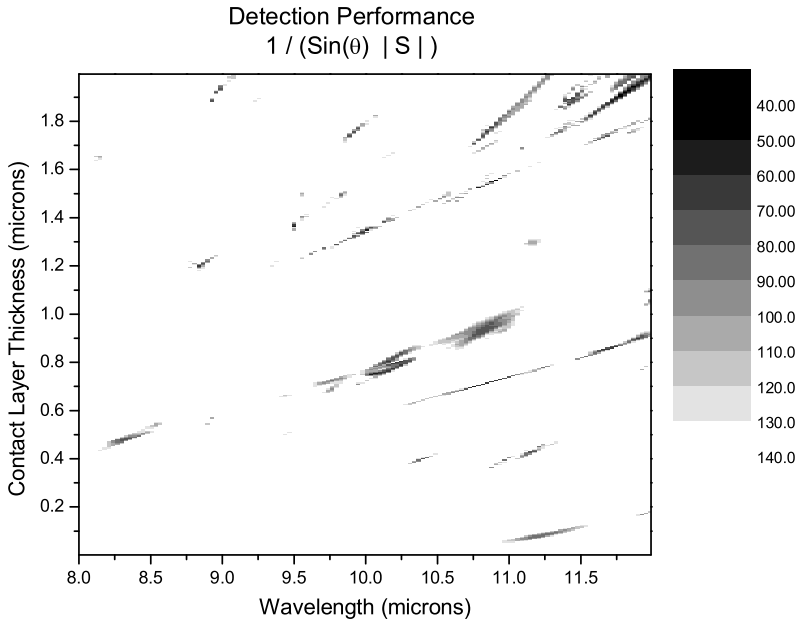

Figure 8. The polarization detection performance for the pixel polarimeter as one varies the wavelength and the thickness of the contact layer between the quantum-wells and the gratings.

Fig. 7 shows how the polarization detection sensitivity changes as I vary the wavelength and the width of the dielectric grooves in all four gratings. In fig. 7 the computer simulation becomes unstable for small groove widths and large wavelengths. Under these circumstances, not enough light penetrates through to the deepest MQW stack to maintain a transfer matrix that can be meaningfully inverted.

Fig. 8 shows how the polarization detection sensitivity changes as I vary the wavelength and the thickness of the contact layers above and below each MQW stack. The device's dependence on interference between the grating layers can be inferred from fig. 8. As you vary the contact layer thickness by δ you change the distance between the gratings by 2δ and the round-trip path-length difference by $4\,m\,\delta$ where m is a positive integer representing interference from layer m. The constructive or destructive interference is caused by two paths for light with an optical phase difference Φ that changes with δ and λ in the following manner:

$$\Phi = \frac{\sqrt{\epsilon_{\mathrm{GaAs}}}\,2\pi}{\lambda}\,4\,m\,\delta = n\,\pi \tag{8}$$

where n is an integer. The constructive or destructive interference may be maintained if we change the contact layer thickness and the wavelength in such a way the Φ is held constant. For constructive interference features, n is even. For destructive interference features, n is odd. In order to detect the polarization, interference is needed from some round trip between gratings at different orientations. Full polarization detection requires interference from all four gratings.

We can compare the slope of the trends on fig. 8 to Eq. (8) by solving for δ:

$$\delta = \frac{n}{8\,m\,\sqrt{\epsilon_{\mathrm{GaAs}}}}\lambda \tag{9}$$

In our code, $\sqrt{\epsilon_{\mathrm{GaAs}}} = 3.28$. For interference between the first and fourth grating, $m = 3$. For contact layer thickness around 0.5 μm the distance between gratings is about 2.75 μm. Recall the grating depth is 0.3 μm.

This means the actual distance traversed across the four gratings is nearly $3.05\mu m \times 6$. Because the wavelength of 10 μm radiation in GaAs is about 3 μm, the phase must advance about $6 \cdot 2\pi$ during the round trip across the four gratings. From the distance traversed we determine the choices of n to be $n = 12$ for constructive interference and $n = 11$ or 13 for destructive interference. A choice of $n = 13$ and $m = 3$ gives a slope of 0.165. The slope of the thin line near 10.5 μm and a contact thickness of $0.5\mu m$ is 0.166. This analysis can be repeated for the other clearly defined lines in fig. 8 to discover which interference paths dominate the polarization detection for the various wavelengths and contact layer thicknesses.

6. DISCUSSION AND CONCLUSIONS

The computer simulation of the pixel-polarimeter demonstrates the potential for full-polarimetric detection in a single pixel using quantum wells. Although our discussion has focused on the LWIR there are potential quantum well structures with effective polarization selection rules with peak-absorption wavelengths of $4-5$ μm or shorter.

The advantages of this new device include (a) polarimetric and hyperspectral information without loss of spatial or spectral resolution compared to a conventional push-broom imaging grating spectrometer (b) no moving parts and most importantly (c) perfect pixel registration in space and time.

The next formidable challenge is to build the device. The semiconductor processing is similar to the processing performed by Lin, Flemming, Yamamoto, and Noda.[17,18] We anticipate the approach of wafer-fusion will be more successful for building the pixel-polarimeter because the quantum-wells will each be grown on a perfect substrate and then gratings will be etched and finally joined. The contacts will be similar to that of a multi-color QWIP.[13] In short, the component technologies have been demonstrated and fabrication is feasible.

ACKNOWLEDGMENTS

I would like to thank D. Cardimona, D. Huang, C. Morath, B. Klemme, P. Alsing, T. Apostalova, D. Le, H. Norton, and L. Evans for many hours of fun and useful discussions and for their comments on the manuscript.

REFERENCES

1. F. Sadjadi and C. Chun, "Machine recognition of objects using ir polarimetry," *SPIE* **2756**, pp. 53–59, 1996.
2. S. Sposato, M. Fetrow, K. Bishop, and T. Caudill, "Two long-wave infrared spectral polarimeters for use in understanding polarization phenomenology," *Optical Engineering* **41**, pp. 1055–64, 2002.
3. J.Holloway, N. Witherspoon, N. Miller, K. Davis, H. Suiter, and R. Hilton, "Navy/marine corps innovative science and technology developments for future enhanced mine detection capabilities," *SPIE* **4038**, pp. 1280–91, 2000.
4. M. Born and E. Wolf, *Principles of Optics*, Pergamon Press, New York, 1975.
5. J. Peterson, G. Jensen, and J. Kristl, "Imaging polarimetry capabilities and measurement uncertainties in remote sensing applicaitons," *SPIE* **4133**, pp. 221–232, 2000.
6. D. Beekman and J. V. Anda, "Polarization sensitive QWIP thermal imager," *Infrared Physics and Technology* **42**, pp. 323–328, 2001.
7. F. Iannarilli, S. Jones, H. Scott, and P. Kebabian, "Polarimetric-spectral intensity modulation (P-SIM): Enabling simultaneous hyperspectral and polarimetric imaging," *SPIE Conference on Infrared Technology Applications XXV* **3698**, p. 474, April 1999.
8. H. Liu, M. Buchanan, and Z. Wasilewski, "How good is the polarization selection rule for intersubband transitions?," *Applied Physics Letters* **72**, April 1998.
9. B. L. Levine, "Quantum-well infrared photodetectors," *J. Appl. Phys.* **74**(8), p. R1, 1993.
10. R. Petit, "A tutorial introduction," in *Electromagnetic Theory of Gratings*, R. Petit, ed., *Topics in Current Physics*, pp. 1–50, Springer-Varlag Berlin Heidelberg, New York, 1980.
11. Y.-L. Kok and N. Gallagher, "Relative phases of electromagnetic waves diffracted by a perfectly conducting rectangular-grooved grating," *J. Opt. Soc. Am. A* **5**, pp. 65–73, January 1988.

12. E. Palik, *Handbook of Optical Constants of Solids*, Academic Press, New York, 1985.
13. M. Sundaram, S. Wang, M. Taylor, A. Reisinger, G. Milne, K. Reiff, R. Rose, and R. Martin, "Two-color quantum well infrared photodetector focal plane arrays," *Infrared Physics and Technology* **42**, p. 301, 2001.
14. J. Pan and C. Fonstad, "Theory, fabrication and characterization of quantum well infrared photodetectors," *Material Science and Engineering* **28**, pp. 65–147, 2000.
15. J. Y. Andersson and L. Lundqvist, "Near-unity quantum efficiency of AlGaAs/GaAs quantum well infrared detectors using a waveguide with a doubly periodic grating coupler," *Appl. Phys. Lett.* **59**(7), p. 857, 1991.
16. L. Wendler and T. Kraft, "Theory of grating-coupler-assisted infrared spectrscopy of lower-dimensional electron systems: Local optics of anisotropic multilayer systems with grating," *Physica B* **271**, pp. 33–98, 1999.
17. S. Lin, J. Fleming, D. Hetherington, B. Smith, R. Biswas, K. Ho, M. Sigalas, W. Zubrzycki, S. Kurtz, and J. Bur, "A three-dimensional photonic crystal operating at infrared wavelengths," *Nature* **394**, p. 251, July 1998.
18. N. Yamamoto, S. Noda, and A. Chutinan, "Development of one period of a three-dimensional phtonic cristal in the 5 micron wavelength region by wafer fusion and laser beam diffraction pattern observation techniques," *Jpn. J. Appl. Phys* **37**, p. L1052, 1998.